Egypt. J. Chem. **Vol. 67**, No. 7 pp. 361 - 376 (2024)

Egyptian Journal of Chemistry
http://ejchem.journals.ekb.eg/

Deoxygenation of Oleic Acid Using Modified MCM-41 Supported Nickel-Tungstate Catalyst to Produce Renewable Biofuel Liquid Alkanes: Kinetic Study

H. A. Elmawgoud*, M. S. Elmelawy, Sarah S. Selim, Salwa A. Ghoneim, Magd M Badr

Egyptian Petroleum Research Institute, Nasr City, Cairo, Egypt

Abstract

Sulfated zirconia-modified NiW/SZ-MCM-41 and alumina-modified NiW/Al_2O_3-MCM-41 catalysts were prepared and characterized using the wet co-impregnation method. NiW/SZ-MCM-41 had better acidity. The focus was on NiW/SZ-MCM-41, and its performance in the deoxygenation of oleic acid was studied under various operational parameters. Kinetic studies at 375-450°C were done, and the Lingo program was used to correlate oleic acid hydrocracking rates with organic liquid product formation. The results matched the experimental data well. Under optimal conditions, both catalysts produced kinds of paraffin (C5-C17) as primary products. Particularly, the content of light paraffin (≤C15) was notably high, comprising 86.25% with the sulfided NiW/SZ-MCM-41 catalyst and 81.30% with the NiW/Al_2O_3-MCM-41 catalyst. Furthermore, the sulfided NiW/SZ-MCM-41 catalyst exhibited superior physical properties in the hydrocracked product compared to the sulfided NiW/Al_2O_3-MCM-41 catalyst. These findings suggest that NiW/SZ-MCM-41 holds promise as a catalyst for converting waste cooking oil into eco-friendly fuel.

Keywords: Green fuels; MCM-41; Sulfated zirconia; Oleic acid; Hydrocracking

1. Introduction

At present, the global community is confronted with two pressing challenges: escalating environmental degradation and the depletion of fossil fuel reserves. Transportation is essential for any country's social and economic development. The need to find alternative fuels for the transportation sector is of utmost urgency due to its significant contribution to greenhouse gas emissions and the accelerating global oil demand[1, 2]. Biodiesel, also known as fatty acid methyl ester (FAME), stands as one of the world's most commonly utilized biofuels. However, its incorporation into fossil diesel mixtures necessitates engine modifications. FAME primarily comprises highly oxygenated compounds, resulting in several drawbacks, including elevated viscosity, a high pour point, a substantial acid content, a reduced heating value, increased nitrogen oxide (NOx) emissions, and inadequate storage stability[3]. Second-generation biofuels represent a category of paraffinic fuels closely aligned with conventional petroleum fuels, distinguished by their production from renewable biomass resources[4]. Crucially, their production does not interfere with food crop cultivation. Examples of second-generation biofuels encompass lignocellulosic ethanol, generated production does not interfere with food crop cultivation. Examples of second-generation biofuels encompass lignocellulosic ethanol, generated through the hydrolysis and fermentation of lignocellulosic biomass; Fischer-Tropsch (F-T) diesel, produced through F-T synthesis from biobased syngas derived from waste biomass; bio-oil, obtained via the pyrolysis of biomass; hydrotreated vegetable oil (HVO); and deoxygenated hydrocarbon fuels, synthesized through catalytic deoxygenation of straight vegetable oils[5].

*Corresponding author e-mail: hussienmawgoud@yahoo.com.; (Hussien A. Elmawgoud)
EJCHEM use only: Received date 29 November 2023; revised date 29 January 2024; accepted date 25 March 2024
DOI: 10.21608/EJCHEM.2024.250667.8924

Biofuels have emerged as a crucial and sustainable fuel source, playing a significant role in reducing greenhouse gas emissions, enhancing air quality, and discovering new energy resources[6-8]. Used cooking oil and fatty acids derived from food processing have been identified as sustainable feed stocks for biofuel production [9-11]. As a result, there has been a growing interest in research and development over the past decade to optimize biofuel production by identifying the most effective catalysts and optimal operating conditions[12]. Numerous countries are now considering the use of vegetable oils and fats as raw materials to produce green fuels. The properties of triglycerides are influenced by the composition of fatty acids and their arrangement on the glycerol molecule[13-17]. Green Chemistry principles promote the application of heterogeneous catalysis and renewable feedstocks in chemical synthesis. Among the various materials, ordered mesoporous silica such as MCM-41 has gained significant attention due to its high surface area and uniform pore size. Modification of MCM-41 with transition metals offers an effective approach to creating active catalytic sites and anchoring active metals, leading to the design of new catalysts. MCM-41 materialsmodified with Al, Ti, and Zr have shown advantages as supports for hydrodesulfurization (HDS) catalysts[18-24]. Transition metal modification of MCM-41 has proven to be a practical methodology for creating active catalytic sites and enhancing the performance of active metals in recent catalyst designs[20].The kinetics of oleic acid hydrocracking reactions were studied at different temperatures (375-450°C), a pressure of 4 MPa, and using a catalyst concentration of 5 wt.%. The experimental data of C18 formation using the NiW/SZ-MCM-41 catalyst within the temperature range of 375°C to 450°C were investigated using the Lingo program. The main goal of this study is to assess the effectiveness of the sulfideNiW/SZ-MCM-41 and NiW/Al_2O_3-MCM-41 catalysts in generating environmentally friendly fuels. This will be achieved by utilizing oleic acid as a representative compound and waste cooking oil in the production process.

2. Experimental

2.1. Materials

The study utilized the following materials: Tetraethylorthosilicate (TEOS, 98% purity, Aldrich), CetylTrimethyl Ammonium Bromide (CTAB, 98% purity, Aldrich), deionized water, ethanol (99.8% purity Sigma-Aldrich), Zirconyl Chloride (99% purity, Sigma-Aldrich), ammonia (28-30% concentration, Sigma-Aldrich), sulfuric acid (97-99% purity, and ammonium metatungstate hydrate, Sigma-Aldrich).

2.2. Catalyst preparation

The synthetic catalysts of NiW/SZ-MCM-41 and NiW/Al_2O_3-MCM-41 were prepared using the wet co-impregnation method. The physical properties of the NiW/SZ-MCM-41 catalysts are provided in Table 1.

Table 1: Physical properties of the NiW/SZ-MCM-41 catalysts [25]

Catalysts	SBET (m^2/g)	VP (cc/g)	Dp (nm)
MCM-41	1448.66	0.87	2.40
Sulfated zirconia	62.083	0.09	3.81
NiW/SZ-MCM-41	444.48	0.30	2.21

2.2.1. MCM-41 Preparation

The procedure for synthesizing mesoporous material based on MCM-41 silica was carried out as described in reference[26]. Deionized water was stirred while adding a specific quantity of CTAB until the mixture became transparent. Then, ethyl alcohol and ammonia liquid were incorporated into the system.

Subsequently, the mixture was stirred while introducing TEOS. The stirring was continued at room temperature for 3 h. The resultant solid product was obtained through filtration and left to air dry at room temperature for 12 h. To eliminate CTAB from the product, calcination was conducted at 540°C for 9 h.

2.2.2. Amorphous Mesoporous Alumina Preparation

The procedure for preparing amorphous mesoporous alumina was as follows. Initially, a suitable quantity of aluminium isopropoxide was dissolved in 0.15 mol of n-heptane and stirred for 1 min. Then, 0.01 mol of acetic acid was added to the solution and stirred. Following that, 0.03 mol of water and 0.01 mol of CTAB were introduced and magnetically stirred for one hour at a temperature of 25°C. After aging for 24 h at room temperature, the mixture was filtered without any rinsing and dried at 60°C for 24 h, followed by an additional 24 h of drying at 90°C. The resulting material was calcined with a gradual temperature increase of 2°C/min until it reached 600°C.

2.2.3. NiW/(Al_2O_3-MCM-41) Catalyst Preparation

The NiW/(Al_2O_3-MCM-41) catalyst preparation consisted of the following procedures. Mesoporous alumina and MCM-41 were mixed mechanically with a weight ratio of 1:3. The metal content of NiW was achieved by employing the wet co-impregnation method using aqueous solutions of Ni $(NO_3)_2 \cdot 6H_2O$ and $(NH_4)6(H_2W_{12}O_{40}) \cdot xH_2O$, with a composition of 10% Ni and 3% W. The obtained solid was dried and then subjected to a 4 h calcination process at a temperature of 450°C.

2.2.4. Sulfiding of NiW/(Al_2O_3-MCM-41) Catalyst

Before conducting the experiments, the catalyst underwent sulfidation (activation) by utilizing a mixture of dimethyl disulfide (DMDS) in isooctane, with a concentration of 5% DMDS[4].The mixture flowed through the catalyst bed at a rate of 1.5 ml/min, with a hydrogen pressure of 3.0 MP. Initially, the reaction temperature was set at 260°C for 2 h, followed by an increase to 360°C for 4 h[27].

2.3. Catalyst Characterization

The catalyst was characterized using different techniques. X-ray diffraction (XRD) patterns were recorded using a Brucker D8 Advanced Powder X-ray Diffraction instrument. N_2 adsorption studies were conducted at -196°C using a NOVA 3200 Apparatus, USA, to evaluate the solid materials' surface area and pore structure. High-resolution transmission electron microscopy (TEM) was performed using a JEOL JEM 2100 Model apparatus (Japan). Fourier Transform Infrared (FTIR) spectroscopy was carried out using a Nicolet Is-10 FT-IR spectrometer[28]. Thermal gravimetric analysis (TGA) [29] and differential scanning calorimetry (DSC) measurements were conducted simultaneously using an SDT Q600 apparatus (USA). Temperature programmed desorption of Ammonia (TPD) was performed using a CHEMBET 3000 Chemical Absorber instrument (Quantachrom) by JAPAN, INC.

2.4. Hydrocracking Experiments procedures

The hydrocracking experiments were conducted using a high-pressure autoclave (Parr model 4575) with a volume of 500 ml. The autoclave was equipped with a digital controller for precise temperature control Figure 1. The operating conditions for the experiments were as follows: temperature (375, 400, 425, and 450°C), initial hydrogen pressure (2, 4, 6, and 8 MPa), catalyst weight percentage (1, 3, 5, and 7%), and a reaction period of 2 h for each run. The operating conditions were varied one at a time while keeping the remaining parameters constant.Before conducting the primary hydrocracking study on oleic acid, a blank test without a catalyst was performed at 425°C and 4 MPa for 2 h. This test showed minimal conversion of oleic acid, and no C18 hydrocarbons such as octadecane and octadecenes were formed. For the kinetics study, the reaction was conducted at 425°C for different durations of 20, 40, 60, 80, 100, 120, 140, and 180 min,while maintaining a constant stirring rate of 500 rpm. During a typical run, 180 g of the feed sample (oleic acid or waste cooking oil)

was introduced into the reactor and purged with hydrogen four times at various pressures to remove air. The reactor was then pressurized with hydrogen to the desired level. In a typical run, the system underwent heating at a rate of 20°C/min while maintaining a stirring speed of 500 rpm. Once the specified reaction time had elapsed, the reactor was cooled, and the resulting liquid products, comprising organic and aqueous fractions, were collected separately in designated containers. The aqueous phase and catalyst were then separated from the liquid products using a syringe and filtration process. The organic liquid products (OLP) were carefully weighed to determine the OLP yield and stored in glass containers for subsequent analysis. Following each run, the utilized catalyst was removed from the autoclave and rinsed with hexane[4]. Likewise, the inner surface of the autoclave was cleansed using hexane. The dissolved fraction in hexane was categorized as residual oil or unconverted oil. The rinsed catalyst was subsequently dried for one hour at 100°C and regenerated by subjecting it to a nitrogen flow at 500°C for one hour. The weight difference before and after catalyst regeneration was recorded as coke. The conversion and yield are defined according to the following equations (1 and 2):

$$conversion wt\ \% = \frac{feedoil(g) - residualoil(g)}{feedoil(g)}\ 100 \quad (1)$$

$$yield wt = \frac{liquidproduct(g)}{feedoil(g)}\ 100 \quad (2)$$

2.4.1. Reusability study

Once the reaction reached completion, the mixture underwent filtration, resulting in the collection of the solid catalyst[4]. This catalyst was then rinsed with n-hexane and subsequently subjected to oven drying at a temperature of 100°C. Afterward, the catalyst was reused for five consecutive hydrocracking cycles under the optimal reaction conditions, which included a temperature of 425°C, a catalyst concentration of 5 wt.%, a pressure of 40 bar, and a reaction time of 2 hours. The determination of Conversion wt.% and Yield wt.% for both the freshly prepared and the recovered sulphide NiW/SZ-MCM 41 catalyst was carried out.

2.5. Gas chromatography for liquid products

To facilitate the gas chromatography (GC) analysis, the organic liquid products were dissolved in pyridine and silylated using N,O-bis(trimethyl)-trifluoroacetamide (BSTFA) and kept in an oven at 60°C for one hour. The analysis was carried out using an Agilent 7890A GC system equipped with a flame ionization detector (FID). The carrier gas used was nitrogen, and the separation was achieved using an HP-5 column with a length of 30 m, internal diameter of 0.32 mm, and film thickness of 0.25 mm. The following temperature program was employed for the analysis: starting at 50°C for 10 min, followed by a ramp of 4°C/min until reaching 300°C, and main taining this temperature for 20 min.

3. Results and Discussion

3.1. Characterization results

3.1.1. FT-IR analysis of NiW/SZ-MCM 41 Catalysts [24]

FTIR analysis was conducted to identify the functional groups within the NiW/SZ-MCM-41 catalyst. As depicted in Figure 2, a prominent band at 967 cm^{-1} was associated with the asymmetric stretching of Si-O-Zr bonds[27]. Furthermore, a distinct peak at 3417 cm^{-1} was attributed to the stretching of O-H bonds in water, accompanied by an O-H bending feature at 1643 cm^{-1}[30]. The presence of ZrO_2 in MCM-41 was indicated by a faint band at 797 cm^{-1}, corresponding to Si-O stretching. Additionally, a subtle signal at 600 cm^{-1} suggested the existence of ZrO_2 in the material. The presence of Zr-O-Si groups was confirmed by a peak at 445 cm^{-1}, while the absence of a band at 425 cm^{-1} indicated the high dispersion of ZrO_2 within the silica framework.

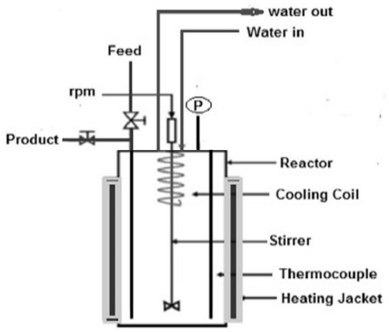

Figure 1: The Reactor Scheme

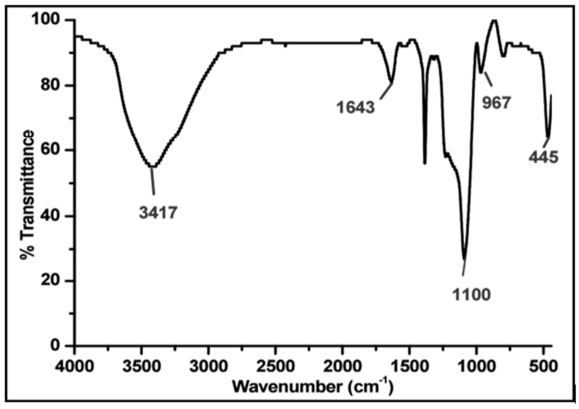

Figure 2: FT-IR Spectroscopy for NiW/SZ-MCM 41 Catalysts

3.1.2. Low Angle XRD of NiW/SZ-MCM-41 Catalysts [24]

Low-angle X-ray diffraction (XRD) analysis was performed to investigate the structural properties of the materials under study. In XRD pattern Figure 3 (MCM-41), displayed a prominent peak at 2.43 degrees, corresponding to the (100) plane reflection lines. This peak is indicative of the organized mesoporous structure of MCM-41 and aligns with the expected hexagonal regularity characteristic of MCM-41 materials in general. In Figure 3b (sulfated zirconia), the XRD pattern for nano-structured exhibited a diffraction peak at 2θ = 2.22 in the low-angle region. This peak underscores the porosity of nano-sulfated zirconia, demonstrating a well-defined pore structure at a short range. Moving to Figure 3 (NiW/SZ-MCM-41), the XRD analysis revealed a peak at 2θ = 2.1 degrees. This observation suggests that the incorporation of sulfated zirconia (SZ) and NiW components led to a partial disruption of the hexagonal ordering within the mesoporous MCM-41 structure, as evidenced by the reduction in peak intensity.

3.1.3. Field Emission Scanning Electron Microscopy (FE-SEM)[24]

Figure 4 presents FE-SEM images showcasing distinct materials. The image exhibits synthesized mesoporous silica MCM-41, revealing a consistent spherical shape, uniform size, and a pristine surface. In contrast, the image displays sulfated zirconia, which displays a remarkable surface shine post-sulfation, likely attributed to the presence of highly charged SO_4- ions. Moving on to the image in Figure 4, we observe the SEM of the NiW/SZ-MCM-41 catalyst. These images affirm the effective impregnation of $SZrO_2$ crystals and NiW oxides onto the surface of the spherical MCM-41 material.

3.1.4. Nitrogen adsorption-Desorption Isotherms of Amorphous Mesoporous Alumina

The nitrogenphysisorption isotherms of amorphous mesoporous alumina were analyzed to obtain information about its porosity and textural properties. Table 2 shows the physical properties of amorphous mesoporous alumina. The isotherms exhibited a distinctive IUPAC type IV shape,which is a characteristic commonly observed in mesoporous materials. Figure 5 shows the isotherm, which displayed a hysteresis loop in the relative pressure range of 0.4 to 0.95. This hysteresis loop suggests the presence of mesoporous channels within the material. The determined BET surface area of the amorphous mesoporous alumina was found to be 295 m^2/g. These findings are consistent with previous research[31].

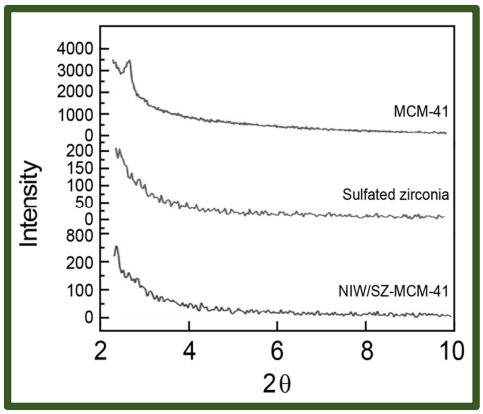

Figure 3: Low Angle XRD of the MCM-41, Sulfonatedzirconia, and NiW/SZ-MCM-41 Catalysts

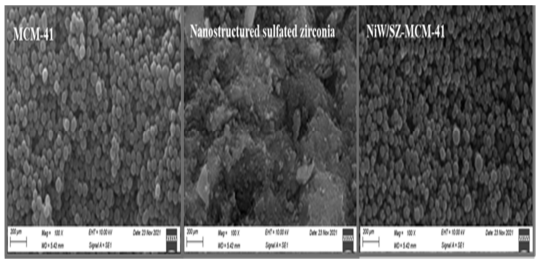

Figure 4: FE-SEM images: for MCM-41, nanostructured sulfated zirconia, and NiW/SZ-MCM-41 catalyst at lower and higher magnification

3.1.4. Nitrogen adsorption-Desorption Isotherms of Amorphous Mesoporous Alumina

The nitrogen physisorption isotherms of amorphous mesoporous alumina were analyzed to obtain information about its porosity and textural properties. Table 2 shows the physical properties of amorphous mesoporous alumina. The isotherms exhibited a distinctive IUPAC type IV shape,which is a characteristic commonly observed in mesoporous materials. Figure 5 shows the isotherm, which displayed a hysteresis loop in the relative pressure range of 0.4 to 0.95. This hysteresis loop suggests the presence of mesoporous channels within the material. The determined BET surface area of the amorphous mesoporous alumina was found to be 295 m^2/g. These findings are consistent with previous research[31].

Table 2: Physical properties of amorphous mesoporous alumina

Support	SBET (m^2/g)	VP (cc/g)	Dp (nm)
Mesoporous alumina	294.947	0.5974	8.10192

Where Dp is the pore diameter, Vp is the pore volume and SBET is the surface area

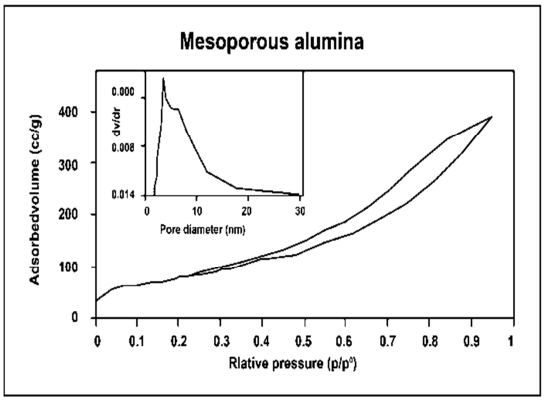

Figure 5: Adsorption-desorption isotherms and pore size distribution for mesoporous alumina

3.1.5. Fourier Transform Infrared (FTIR) of amorphous mesoporous alumina

The FTIR spectrum of amorphous mesoporous alumina revealed significant absorption bands. At 3510 cm^{-1}, a broad band was observed, which corresponds to physisorbed and coordinated water. This band is accompanied by a band at 1664 cm^{-1}, which is attributed to the bending mode (υHOH) of coordinated water. Additionally, two prominent peaks were observed at 1486 cm^{-1} and 687 cm^{-1}, corresponding to the symmetric and asymmetric stretching of the Al-O-Al bond, respectively. These peaks can be assigned to the amorphous mesoporous alumina framework. Refer to Figure 6 for the FTIR spectrum.

3.1.6. Low Angle X-ray Diffraction of NiW/Al_2O_3-MCM-41catalyst

The XRD pattern for NiW/Al_2O_3-MCM-41 composite shown in Figure 7 features a distinct peak at 2Θ attenuated 2.22, which can be indexed as (100) reflections of hexagonal mesoporous structure.

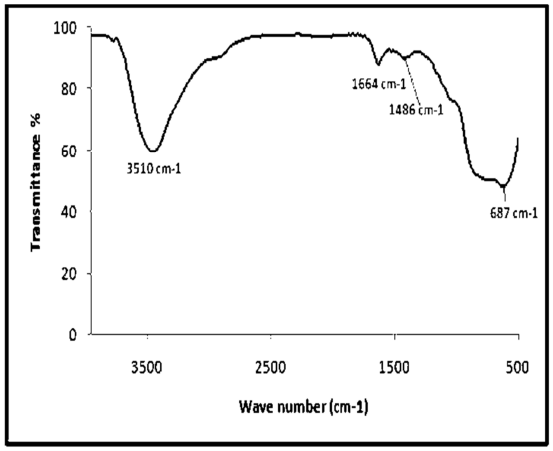

Figure 6: FT-IR of amorphous mesoporous alumina

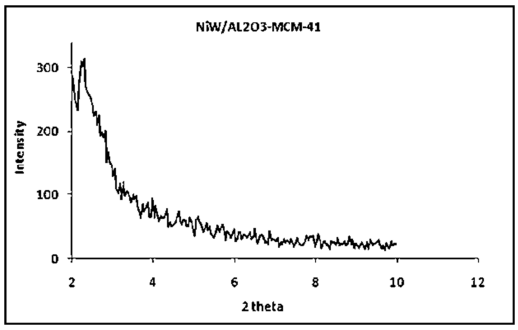

Figure 7: XRD of NiW/Al_2O_3-MCM-41 composite

3.1.7. Adsorption-Desorption Isotherms of NiW/Al_2O_3-MCM-41 Catalyst

The nitrogen physisorption isotherms of the NiW/Al_2O_3-MCM-41 catalyst were examined to assess its porosity and textural properties. Table 3 shows the physical properties of the NiW/Al_2O_3-MCM-41 catalyst.Figure 8 demonstrates a noticeable shift in the isotherm about p/p° (0.43-0.93), indicating the presence of both micro and mesostructures in the composite. The catalyst demonstrated a BET surface area of 514.663 m^2/g and a total pore volume of 0.13 cm^3/g.

Table 3: Physical properties of NiW/Al_2O_3-MCM-41catalyst

Catalyst	SBET (m^2/g)	VP (cc/g)	Dp (nm)
NiW/Al_2O_3-MCM-41	514.663	0.13	3.82

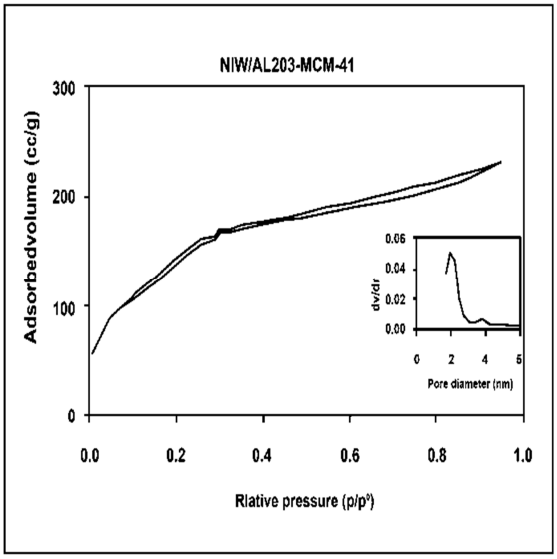

Figure 8: Adsorption-desorption isotherms and pore size distribution

3.1.8. High-Resolution Transmission Electron Microscope (HRTEM)

The high-resolution transmission electron micrographs shown in Figure 9 (a, b, and c) depict the NiW/Al_2O_3-MCM-41 catalyst. The images exhibit a well-defined hexagonal arrangement of uniform channels, suggesting a highly organized pore structure. This suggests the absence of bulk aggregation both inside and outside the pores.

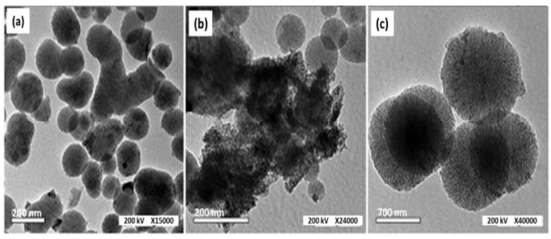

Figure 9: TEM images (a, b, and c) for amorphous mesoporous alumina at lower and higher magnification

3.1.9. Thermal Analysis

Thermal analysis of the NiW/Al_2O_3-MCM-41 catalyst was conducted using TGA (thermogravimetric analysis) and DSC (differential scanning calorimetry) in the temperature range of 35-550°C. As shown in Figure 10, the TGA and DSC curves revealed weight losses occurring below

550°C, with no further weight loss observed thereafter. The initial weight loss of approximately 10% at temperatures below 100°C, accompanied by an exothermic peak peaking at 62°C, can be ascribed to the elimination of physically adsorbed water. Subsequently, the sample exhibited stability up to 550°C. Overall, the catalyst exhibited high thermal stability up to 550°C.

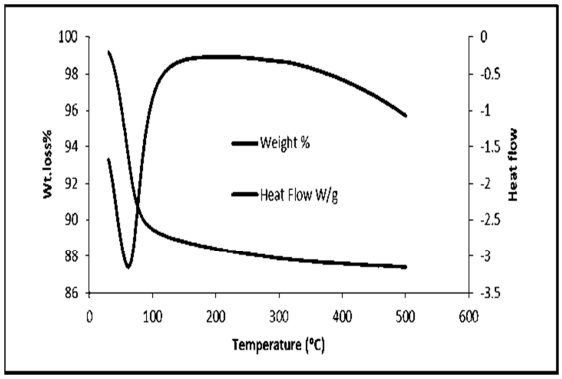

Figure 10: TGA & DSC for NiW/Al_2O_3-MCM-41 catalyst

3.1.10. Temperature Programmed Desorption

Temperature programmed desorption (TPD) of adsorbed ammonia was employed to measure the acidic intensity of the catalyst. The peaks at 200°C illustrate weak acidic sites, while the signals at 500°C show strong acidic sites. The peak at 800°C might be due to phase transitions. Peaks in high-temperature areas may be related to the desorption of ammonia from strong Lewis and Bronsted sites which are important in catalysis applications. The signal at lower temperatures is called a symmetric peak, while the peak at higher temperatures is named an asymmetric peak. The asymmetric peak can be divided into two peaks. If the asymmetric peak was large, this related to desorption from a strong Bronsted acid site. If the asymmetric signal was small, this indicated the desorption from a strong Lewis site. For the NiW/SZ-MCM-41 catalyst, Figure 11(a) indicates the presence of weak acid sites at 150°C and very strong acid sites at 550°C. On the other hand, for the NiW/Al_2O_3-MCM-41 catalyst shown in Figure 11(b), weak acid sites are observed at 104°C, and strong acid sites are observed at 514°C. This result suggests that the NiW/SZ-MCM-41 catalyst exhibits better acidity compared to the other catalysts.

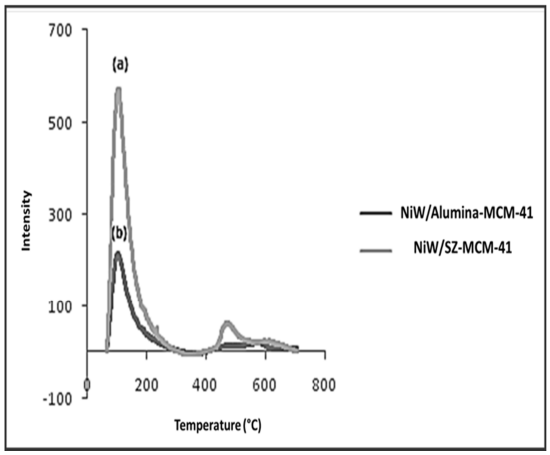

Figure 11: TPD of NiW/SZ-MCM-41 catalyst and NiW/Al_2O_3-MCM-41 catalyst

3.1.11. Catalyst stability studies

The stability of the sulphide NiW/SZ-MCM 41 catalyst was assessed under the optimal reaction conditions: a temperature of 425°C, a catalyst concentration of 5 wt.%, a pressure of 40 bar, and a reaction time of 2 h. Throughout multiple cycle runs, a slight decrease in catalytic activity was observed. Initially, the conversion of oleic acid and the yield of the organic liquid products (OLP) products were both maintained at approximately 94.81 wt.% and 73.40 wt.%, respectively. After five consecutive catalytic runs, these values showed a marginal reduction to 88.53% and 68.82%, respectively. This decline in deoxygenation activity could be attributed to the deposition of coke and/or the irreversible adsorption of large oleic acid molecules, which may lead to gum formation within the catalyst pores. Nevertheless, it highlights the overall higher stability of the

sulfideNiW/SZ-MCM 41 catalyst following the specified duration of catalytic runs.

3.2. Oleic acid deoxygenation utilizing NiW/SZ-MCM-41 catalyst

The deoxygenation of oleic acid was investigated using the NiW/SZ-MCM-41 catalyst to assess the influence of different operating conditions on the characteristics of the resulting products. Among the various operating factors, some significant parameters, such as reaction temperature, catalyst amount, and reaction pressure, influence the deoxygenation process and the hydrocarbon products[5].

3.2.1. Effect of temperature on the deoxygenations of oleic acid

The impact of temperature on both the yield and quality of the hydrocracked products of oleic acid, employing the sulphide NiW/SZ-MCM-41 catalyst, was assessed at various temperatures, i.e., 375°C, 400°C, 425°C, and 450°C; the remaining operating conditions were kept constant (p: 2 MPa, 3 wt.% catalyst, and 2 h). As indicated in Table 4. The organic liquid product (OLP) decreases from 73.9% at 375 °C to 60.28% at 450°C. As the reaction temperature increases, the gas yield gradually increases from 5.87% at 375°C to 25.48% at 450 °C. The increasing severity of the reaction conditions led to the decomposition of oleic acid, producing low molecular weight gases. The yield of the Residue gradually decreases from 14.07% at 375°C to 6.13% at 450°C. We noticed that with increasing temperature, the conversion increases because, under the hydrocracking conditions, as the temperature increases, the severity of the reaction conditions intensifies, leading to more vigorous interactions between the molecules of oleic acid and the hydrogen gas at the active sites of the sulfideNiW/ZS-MCM-41 catalyst. The data illustrated in Table 4 also indicate that increasing the temperature to 450°C resulted in the gradual improvement of the properties of the hydrocracked product, as the density dropped to 0.8576 with a significant reduction in viscosity to 2,88 cSt in addition to improvement in pour point (-39°C), total acid number (0.031) and calorific value (42.83). As expected, the gaseous products increased substantially with temperature. They were associated with a slight drop in the OLP due to the sulfideNiW/SZ-MCM-41 catalyst, which incorporates sufficient strong acid centers. The presence of water during the temperature range of the deoxygenation process suggests that the reaction proceeds through decarbonylation and hydrodeoxygenation pathways. Therefore, a reaction temperature of 425°C could be regarded as the most suitable temperature for deoxygenation of the oleic acid as it gives satisfactory conversion with an appropriate yield of OLP. Moreover, the product is distinguished by an excellent pour point, calorific value, total acid number, and good flash point.

Table 4: Properties of Bio-Crude Products from the Conversion of oleic acid over NiW/SZ-MCM-41 at 20 bars, 3 wt.% catalyst, 2 h and 375, 400, 425, and 450°C

Properties	375˚C	400˚C	425˚C	450˚C	Method
Density at 20˚C.g/cm^3	0.8733	0.8598	0.8580	0.8576	ASTM D-1298
Kinematic visc. \cStat 40˚C	4.5	3.15	3.06	2.88	ASTM D-445
Total acid no., mg KOH/gm	0.072	0.056	0.034	0.031	ASTM D-664
Calorific value KJ/Kg	40.98	41.49	42.70	42.83	ASTM D-240
Flash point ˚C	121	96	68	65	ASTM D-92
Pour point ˚C	-21	-27	-39	-39	ASTM D-97
Sulfur wt.%	Nil	Nil	Nil	Nil	ASTM D-129
Conversion wt.%	85.92	89.32	92.14	94.76	-
Gas yield wt.%	5.87	18.05	24.66	25.48	-
OLP wt.%	73.9	67.04	65.71	60.28	-
Residue wt.%	14.07	10.68	7.86	6.13	-
Water wt.%	4.76	2.02	1.19	5.72	-
Coke wt.%	1.40	1.61	0.58	2.39	-

3.2.2. Effect of catalyst quantity on the deoxygenations of oleic acid

The amount of catalyst utilized in the deoxygenation process of oleic acid plays a crucial role in determining the efficiency and effectiveness of the reaction. Table 5 shows that increasing catalyst wt.% (1, 3, 5, and 7) positively affects oleic acid conversion. Oleic acid conversion rose from 93.33% (at 1 wt.% catalyst) to 96.81% (at 7 wt.% catalyst.). Increasing the catalyst quantity provides a greater number of active sites, which can enhance the reaction efficiency and promote higher conversion rates[32]. Table 5 shows the organic liquid product decreased from 71.83% at 1 wt.% to 65.71% at 3 wt.% and then increased to 75.14% at 7 wt.%. As the catalyst wt.% increased, the gas yield increased from 19.22% at 1wt.% to 24.66 at 3wt.% and then decreased to 16,95% at 7 wt.%. The yield of the Residue decreases from 6.66% at 1 wt.% to 5.42% at 7 wt.%. It can be demonstrated the slight Effect of sulfided NiW/SZ- MCM 41 catalyst quantity on OLP yield between 5% and 7% catalyst was observed.

Table 5: Properties of bio-crude products from the conversion of oleic acid over SulfideNiW/SZ-MCM-41 at, 20 bar, 425ºC, 2 h, and catalyst 1, 3, 5, and 7 wt.%

Properties	1%	3%	5%	7%	Method
Density at 20°C.g/cm^3	0.8811	0.8570	0.8673	0.866	ASTM D-1298
Kinematic viscosity cSt at 40°C	3.34	3.06	3.06	3.02	ASTM D-445
Total acid no., mg KOH/gm.	0.08	0.034	0.035	0.041	ASTM D-664
Calorific value KJ/Kg	40.57	42.70	43.66	43.18	ASTM D-240
Flash point °C	91	68	75	73	ASTM D-92
Pour point °C	-41	-39	-39	-45	ASTM D-97
Sulfur wt.%	Nil	Nil	Nil	Nil	ASTM D-129
Conversion wt.%	93.33	92.14	94.27	96.81	
Gas yield wt.%	19.22	24.66	19.44	16.95	
OLP wt.%	71.83	65.71	74.08	75.14	-
Residue wt.%	6.66	7.86	5.73	5.42	-
Water wt.%	1.78	1.19	0.52	1.85	-
Coke wt.%	0.51	0.58	0.23	0.64	-

A slight viscosity and flash point variation is noticeable at 5 wt.% and 7 wt.%. From the above data, 5 wt.% can be considered the best catalyst quantity under the same conditions.

3.2.3. Effect of pressure on the deoxygenations of oleic acid

In the deoxygenation process, the presence of hydrogen is often necessary to prevent catalyst deactivation and preserve the activity of the catalysts. Hydrogen plays a crucial role by scavenging the surface of the catalyst from deactivating species[33].

The Effect of pressure on hydrocracked product phase yields is illustrated in Table 6. A slight decrease in OLP yield was observed by increasing the pressure from 20 bar to 80 bar. This may be due to the hydrodeoxygenation mechanism (HDO) being favored at higher pressure; this, however, produces more water as well, which may deactivate the catalyst and reduce the yield of the OLP product. At the same time, Residue and gas are slightly affected by the increasing pressure. The data show that the 4 MPa is regarded as the preferable pressure applied here since it gives low viscosity (2.4 cSt) and a good conversion of OLP (94.81%) that is characterized by a suitable pour point (-33°C) and flash point (75°C). Therefore, according to the data mentioned, the highest conversion and the lowest viscosity can be achieved at 4 MPa hydrogen pressure. Hence, the hydrogen pressure of 4 MPa can be considered the best hydrogen pressure for economic purposes. According to the above discussions, it can be seen that temperature at 425°C, catalyst 5 wt.%, pressure 4 MPa, and 2 h are the most suitable experimental conditions for hydrocracking the oleic acid on sulphide NiW/SZ-MCM-41 catalyst.

Table 6: Properties of bio-crude products from the conversion of oleic acid over SulfidedNiW/SZ-MCM-41 at5 wt.%

Properties	20 bar	40 bar	60 bar	80 bar	Method
Density at 20°C.g/cm^3	0.867	0.865	0.861	0.868	ASTM D-1298
Kinematic viscosity cSt at 40°C	3.06	2.4	4.23	4.28	ASTM D-445
Total acid no., mg KOH/gm	0.047	0.035	0.062	0.035	ASTM D-664
Calorific value KJ/Kg	43.66	40.66	43.97	43.12	ASTM D-240
Flash point °C	75	75	81	85	ASTM D-92
Pour point °C	-39	-33	-25	- 20	ASTM D-97
Sulfur wt.%	Nil	Nil	Nil	Nil	ASTM D-129
Conversion wt.%	94.27	94.81	94.27	92.35	-
Gas yield wt.%	19.44	20.73	21.80	24.16	-
OLP wt.%	74.08	73.40	72.96	70.81	-
Residue wt.%	5.73	5.19	3.60	3.10	-
Water wt.%	0.52	0.47	1.41	1.68	-
Coke wt.%	0.23	0.21	0.23	0.25	-

3.3. Kinetics study

The kinetic modeling results led to the proposal of reaction schemes for the hydrodeoxygenation process. Equations (3-10) represent the mass balance and reaction kinetics, along with their corresponding reaction routes and rate constants (k values) with confidence intervals. The kinetics of oleic acid hydrocracking reactions were studied at different

temperatures (375-450°C), a pressure of 4 MPa, and using a catalyst concentration of 5 wt.%.

It should be noted that the hydrodeoxygenation of oleic acid typically proceeds through sequential hydrogenation, saturating the double bonds to form stearic acid (SA). As a result, the direct formation of the C18 biofuel may not be readily feasible, and the corresponding rate constant (k1 in Scheme 1) can be set to zero, consequently, the following sets of differential equations (3-10) were obtained.

$$-\frac{dC_{OA}}{dt} = k_2 C_{OA} \quad (3)$$

$$\frac{dC_{SA}}{dt} = k_2 C_{OA} - k_3 C_{SA} \quad (4)$$

From equation (3)

$$C_{OA} = C_{OA_0}.e^{-(k_2)t} \quad (5)$$

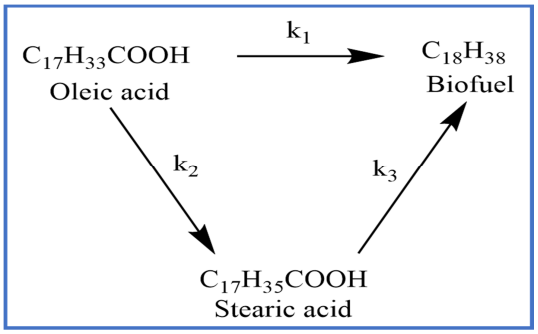

Scheme 1: Possible reaction pathways for deoxygenation of oleic acid

Substituting Eq. (5) into Eq. (4) gives Eq. (6), which upon integration with boundary limits:

When: $t = 0,\ C_{OA} = C_{OA_0}$ and $C_{SA} = C_{SA_0} = 0$

Gives rise to Eq. (7).

$$\frac{dC_{SA}}{dt} = k_2 C_{OA_0}.e^{-(k_2)t} - k_3 C_{SA} \quad (6)$$

$$C_{SA} = \frac{k_2 C_{OA_0}}{(k_3 - k_2)} \quad [e^{-(k_2)t} - e^{-(k_3)t}] \quad (7)$$

By substituting Equations (5) and (7) into Equation (8), the formation of C18 biofuel can be determined. Both n-$C_{18}H_{38}$and iso-$C_{18}H_{38}$ are combined as C18 since they have the same molecular formula and weight.

$$\text{i.e} C_{18} = C_{OA_0} - C_{OA} - C_{SA} \quad (8)$$

By rearranging Equation (9), Equation (10) is obtained, which establishes a relationship between the production of C18 biofuel and the initial concentration of oleic acid as a function of reaction time.

$$C_{18} = C_{OA_0} - C_{OA_0}e^{-(k_2)t} - \frac{k_2 C_{OA_0}}{(k_3 - k_2)} \quad [e^{-(k_2)t} - e^{-(k_3)t}] \quad (9)$$

$$\frac{C_{18}}{C_{OA_0}} = \frac{1}{(k_3 - k_2)}\left[k_3[1 - e^{-(k_2)t}] - k_2[1 - e^{-(k_3)t}]\right] \quad (10)$$

The experimental data for C18 formation using the NiW/SZ-MCM-41 catalyst at temperatures ranging from 375°C to 450°C were fitted to Equation (10) using the Lingo program[34]. The resulting plots, illustrated in Figure 12, exhibited a reasonable level of correlation between the experimental and developed models, with observed R^2 values of 0.975, 0.963, 0.955, and 0.948 for temperatures of 375°C, 400°C, 425°C, and 450°C, respectively.

$$R^2 = 1 - \frac{(C_{exp} - C_{est})^2}{(C_{exp} - \acute{c}_{exp})^2} \quad (11)$$

Furthermore, the production of C18 biofuel increased with longer reaction times and higher temperatures (Figure 12).

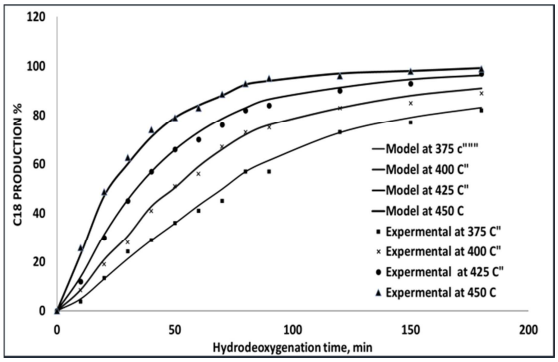

Figure 12: Experimental data fitting of the HDO of oleic acid at 5 wt.% catalyst and 4 MPa pressure

The estimated results were compared with the experimental data, and a good agreement was observed, as indicated by the calculated R^2 values. Table 7 provides a summary of this comparison.

Table 7: Comparison between the experimental and estimated results at different temperatures

Parameter	375°C		400°C		425°C		450°C	
	Est	Exp	Est	Expt	Est	Expt	Est	Expt
Conversion wt.%	81	85.9	85.3	89.32	89.1	92.1	92.1	94.76
Gas wt.%	8.43	5.87	20.6	18.05	27.7	24.6	32.1	25.48
OLP wt.%	69.9	73.9	63.2	67.04	61.8	65.7	58.8	60.28
Residue wt.%	15.8	14.0	10.0	10.68	6.89	7.86	5.6	6.13
Water wt.%	3.9	4.76	1.9	2.02	1.54	1.19	1.32	5.72

The effect of reaction time on the hydrodeoxygenation (HDO) of oleic acid using the NiW/SZ-MCM-41 catalyst was investigated. The product distribution profile as a function of HDO time is shown in Figure 13. It can be observed that as the reaction progressed, stearic acid (SA) was formed and reached its peak formation at around 20 min of reaction time. However, after 50 min of reaction time, the formation of SA started to decrease. This is because the hydrodeoxygenation of unsaturated compounds proceeds through sequential hydrogenation to saturate the double bonds, followed by deoxygenation.

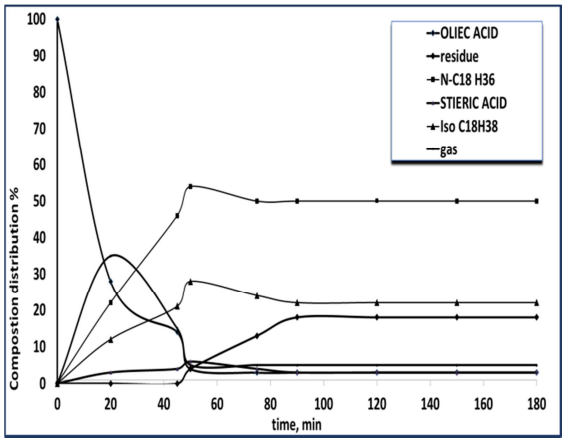

Figure 13: Effect of time on the HDO of oleic acid into biofuel at 425°C, 4 MPa, and 5wt.% catalyst

The yield of both normal and isomerized octadecane (n-$C_{18}H_{38}$ and iso-$C_{18}H_{38}$), which are considered the main fractions, increased progressively until reaching a maximum at 50 min of reaction time, with yields of approximately 54% and 28%, respectively. The presence of isomerized products can be attributed to the acidity of the catalyst. At 75 min of HDO time, the yield of the main products started to decrease, possibly due to the prevalence of specific secondary reactions such as cracking and oligomerization. This was evidenced by an increase in the number of gases produced. After 180 min, oligomerization reactions became more prevalent, as indicated by an increase in the fraction of residue from approximately 4% at 50 min to 23%, while the fraction of gases decreased. The estimated rate constants for the HDO of oleic acid are presented in Table 8. The results showed that the effect of temperature on the kinetics of the HDO process follows the Arrhenius theory, which describes the temperature dependence of reaction rates. It is also observed that the sequential hydrogenation of oleic acid to form stearic acid (k2) is favored and faster compared to the eventual formation of C18 biofuel (k3), indicating that the deoxygenation step is the rate-controlling step. For all four temperatures studied, the rate constant for the hydrogenation of oleic acid (k2) is much higher than the deoxygenation rate constant (k3), indicating that deoxygenation is the rate-limiting step at all investigated temperatures. Moreover, with an increase in reaction temperature, all the rate constants increase as well.

Table 8: Estimated parameters at different temperatures

parameters	375ºC	400ºC	425ºC	450ºC
k_2 (S^{-1})	0.372	0.424	0.482	0.523
k_3 (S^{-1})	0.0464	0.0521	0.063	0.0672

3.4. Hydrocracked waste cooking oil (WCO)

The composition of WCO indicates that it has a high density (0.9239), viscosity (38.02), and acid value (4 mg. KOH/g. oil), demonstrating that it contains free fatty acids. The physicochemical characteristics of

hydrocracked products from the conversion of waste cooking oil over sulfideNiW/SZ-MCM 41(hydrocracked Product 1) &sulfidedNiW/Al_2O_3-MCM-41 (hydrocracked Product 2) at 425ºC, 5 wt.% catalyst, 40 bar for 2 h were illustrated in Table 9. Furthermore, Table 9 provides a summary of the physicochemical properties of Waste Cooking Oil (WCO) in comparison to petroleum diesel, and the Biodiesel standard[12].

The represented data demonstrated the crucial improvement in the quality of the obtained hydrocracked product using NiW/SZ-MCM-41 compared to NiW/ϒ-Al_2O_3–MCM-41, as observed from the data. It is noticed that a distinct reduction of the density to 0.8431 and 0.8491 gm/cm^3 for NiW/SZ-MCM-41 &NiW/ϒ-Al_2O_3–MCM-41, respectively. As well as an enormous drop in viscosity to 2.61 and 2.86 cSt, this may be due to breaking the triglyceride molecules in WCO into smaller fragments that are much less viscous than the parent oil. Furthermore, a marked improvement in the pour point dropped to -19ºC and -15ºC for hydrocracked products, respectively. The flash point of the obtained product is entire and amounts to 135ºC and 140ºC, confirming the fuel's safety to the handle during operation or storage.

The calorific value of the product obtained from the HDO of the waste cooking oil using the NiW/SZ-MCM-41 catalyst was determined to be 43.96 kJ/kg. This value is higher compared to the calorific value of 42.02 kJ/kg obtained from the NiW/Al_2O_3-MCM-41 catalyst. The increase in calorific value can be attributed to the reduction in the number of oxygenated compounds, such as fatty acids, present in the product. The shallow values of the acid number indicated that the products did not contain any free acids. The obtained result suggests that all the cracked products exhibited no corrosion (1a Effect). The cetane index is a measure of the ignition quality of diesel fuel, specifically related to its ignition delay period in a diesel engine[35]. Based on the results obtained, it is observed that the hydrocracked products obtained using the NiW/SZ-MCM-41 catalyst possesses a good cetane index compared to the NiW/Al_2O_3-MCM-41 catalyst. In addition, the obtained data closely aligns with the ASTM standards for both biodiesel and petroleum diesel, as shown in Table 9.

Table 9: Properties of the Hydrocracked Products from the Conversion of Waste Cooking Oil Over SulfidedNiW/SZ-MCM-41(1) &NiW/ϒ-Al_2O_3–MCM-41(2) at 425ºC, 5 wt.% Catalyst and 40 MPa, 2 h, as Compared with That of The Petroleum Diesel and The Biodiesel Standard, (USA).

Properties	Feed (WCO)	Hydro-cracked Product (1)	Hydro-cracked Product (2)	Biodiesel standard, ASTM D6751-07b	Petroleum diesel	Method
Density at 20˚C.g/cm^3	0.9239	0.8431	0.8491	-	0.820 to 0.845[b]	ASTM D-1298
Kinematic visc. cSt at 40˚C	38.02	2.61	2.86	1.9 to 6	2 to 4.5	ASTM D-445
Total acid no., mg KOH/gm.	4	0.07	0.34	0.50 maximum	-	ASTM D-664
Calorific value KJ/Kg	2035	43.96	42.02	-	45.5 MJ/kg	ASTM D-240
Flash point ˚C	230	135	140	93 minimum	55 minimum	ASTM D-92
Pour point ˚C	-6	-19	-15	-15 to 10	-90	ASTM D-97
Sulfur (wt.%)		Nil	Nil			ASTM D-129
Copper stripper corrosion (3h, 50˚C)		1a	1a	1a		ASTM D-130
Cetane index		70	65	47 to 60	51 minimum	ASTM D-976
Conversion (wt.%)		91	90.43			-
OLP (wt.%)		69.81	65			-

Figure 14 and 15 shows the FID-GC charts of liquid hydrocarbons formed from the hydrocracking of waste cooking oil over sulfided NiW/SZ-MCM-41 and sulfided NiW/Al_2O_3-MCM-41 catalysts at the optimum conditions (4 MPa, temp. 425ºC, 5wt.%

catalyst, and 2h). The OLP contains large amounts of normal and iso-paraffins C5-C17 as the main products, and the amounts of light paraffin (≤C15) were very high (86.25%) for sulfidedNiW/SZ-MCM-41catalyst and (81.30%) for NiW/Al_2O_3-MCM-41 catalyst, this may be due to the acidic strength of the sulfided catalysts.

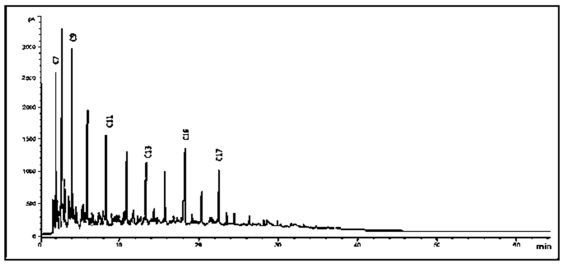

Figure 14: The FID-GC charts of liquid hydrocarbons formed from the hydrocracking of waste cooking oil over sulfided NiW/SZ-MCM-41 catalyst at 4 MPa, temp. 425ºC, 5wt.% catalyst, and 2 h

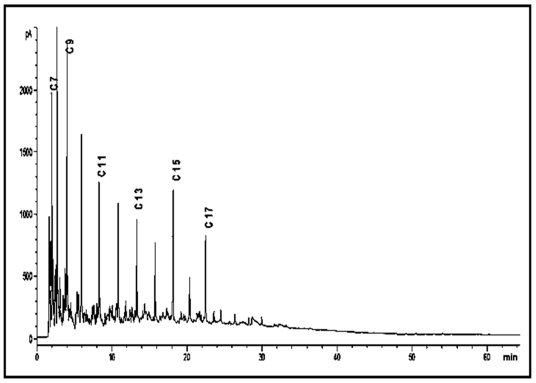

Figure 15: The FID-GC charts of liquid hydrocarbons formed from the hydrocracking of waste cooking oil over sulfided NiW/Al_2O_3-MCM-41 catalyst at 4 MPa, temp. 425ºC, 5wt.% and 2 h

Table 10 presents a comparative analysis of catalytic deoxygenation performance using various feedstocks. The experimental conditions, including temperature, pressure, and hydrocarbon yield, closely resemble those from previous research, enabling a meaningful comparison of results. The findings indicate that the NiW/SZ-MCM-41 catalyst in our study exhibited superior deoxygenation capabilities, yielding 73.40% for oleic acid and 69.81% for waste cooking oil, compatible with the performance of other catalysts[36-39]. The enhanced efficiency of the NiW/SZ-MCM-41 catalyst can be attributed to its robust acidity and the synergistic interaction between the Ni–W components and the SZ-MCM-41 support, in contrast to the NiW/ϒ-Al_2O_3–MCM-41 catalyst.

Table 10: Comparison study of the catalytic deoxygenation activity with various feeds

Catalyst	Feed	Reaction conditions	Hydro carbon Yield (wt.%)	Referen ces
NiW/SZ-MCM-41	Oleic acid	425°C, catalyst 5 wt.%, pressure 4 MPa, and 2 h	73.40	Present study
NiW/SZ-MCM-41	Waste cooking oil	425°C, catalyst 5 wt.%, pressure 4 MPa, and 2 h	69.81	Present study
NiW/ϒ-Al_2O_3–MCM-41	Waste cooking oil	425°C, catalyst 5 wt.%, pressure 4 MPa, and 2 h	65	Present study
NiMo/ɣ-Al_2O_3	waste cooking oil	400C, pressure 60 bar and 4 h	77,97 %	33
20 wt.% ofCaO in BBTPFS catalyst	waste cooking oil	400 °C, H_2 pressure 50 bars, and 1 h	66.29 vol%	34
Mo-Zn/Al_2O_3 catalyst	carinata oil	350 °C, H_2 pressure 300 psi, and 5 h	81.05 %	35
catalyst (Pd/C)	sunflower oil	300°C, H_2 pressure 40 bar, and molar ratio H_2/oil 2.5:1	> 78%.	36

Abbreviations

High-resolution transmission electron microscope (HRTEM)	American Society for Testing and Materials(ASTM)
Hydride oxygenation mechanism (HDO)	Organic liquid products (OLP)
The surface area (SBET)	Fatty acid methyl ester (FAME)
Temperature programmed desorption (TPD)	Nitrogen oxide (NOx)
High-resolution transmission electron microscope (HRTEM)	American Society for Testing and Materials(ASTM)
Gas Chromatography (GC)	Hydrotreated vegetable oil (HVO)
N,O-bis(trimethyl)-trifluoroacetamide (BSTFA)	Temperature-programmed desorption of Ammonia (TPD)

Thermal gravimetric analysis (TGA)	Tetraethylorthosilicate (TEOS)
The pore diameter (Dp)	Dimethyl disulfide (DMDS)
The pore volume, (Vp)	X-ray diffraction (XRD)
Fourier transform infrared (FTIR)	Olic acid concentration, (C_{OA})
Rate constants (k1, k2, k3)	Olic acid concentration at time 0 (C_{OA}
Differential scanning calorimetry (DSC)	Stearic acid concentration at time zer
Stearic acid concentration	Flame ionization detector (FID)

5. Conclusion

The study compared two synthetic catalysts, NiW/SZ-MCM-41 and NiW/Al_2O_3-MCM-41, prepared using wet co-impregnation. Various characterization techniques were employed to evaluate these catalysts, revealing that NiW/SZ-MCM-41 outperformed NiW/Al_2O_3-MCM-41.

Optimal conditions for hydrocracking oleic acid using NiW/SZ-MCM-41 were found to be 425°C, 5 wt.% catalyst loading, 4 MPa pressure, and a 2-hour reaction time. Higher temperatures and longer reaction times increased C18 biofuel production, which is in good agreement with the estimated values obtained using the lingo program. Waste cooking oil hydrocracking with NiW/SZ-MCM-41 yielded a significant amount of normal and iso-paraffins (C5 to C17), with the majority being light paraffins (≤C15).

In comparing physical properties, NiW/SZ-MCM-41 outperformed NiW/Al_2O_3-MCM-41, particularly in deoxygenation capabilities, achieving 73.40% for oleic acid and 69.81% for waste cooking oil. These results suggest that NiW/SZ-MCM-41 is an excellent catalyst for converting waste cooking oil into eco-friendly green fuel.

6. Conflicts of interest

The authors state no conflict of interest regarding this work to declare.

7. Formatting of funding sources

No funding was received for the present work.

8. References

[1] T. Li, Z.-C. Liu, H.-C. Zhang, Q.-H. Jiang, Environmental emissions and energy consumptions assessment of a diesel engine from the life cycle perspective, Journal of Cleaner Production 53 (2013) 7-12.

[2] N.C. Surawski, Z.D. Ristovski, R.J. Brown, R. Situ, Gaseous and particle emissions from an ethanol fumigated compression ignition engine, Energy Conversion and Management 54(1) (2012) 145-151.

[3] N. Hongloi, P. Prapainainar, A. Seubsai, K. Sudsakorn, C. Prapainainar, Nickel catalyst with different supports for green diesel production, Energy 182 (2019) 306-320.

[4] S.A. Hanafi, M.S. Elmelawy, H.A. Ahmed, Solvent-free deoxygenation of low-cost fat to produce diesel-like hydrocarbons over Ni–MoS2/Al_2O_3–TiO_2 heterogenized catalyst, International Journal of Energy and Water Resources 6(1) (2022) 1-13.

[5] B.P. Pattanaik, R.D. Misra, Effect of reaction pathway and operating parameters on the deoxygenation of vegetable oils to produce diesel range hydrocarbon fuels: A review, Renewable and Sustainable Energy Reviews 73 (2017) 545-557.

[6] A. Demirbas, Comparison of transesterification methods for production of biodiesel from vegetable oils and fats, Energy Conversion and Management 49(1) (2008) 125-130.

[7] A. Jaecker-Voirol, I. Durand, G. Hillion, B. Delfort, X. Montagne, Glycerin for New Biodiesel Formulation, Oil & Gas Science and Technology - Revue de l'IFP 63(4) (2008) 395-404.

[8] M.F. Othman, A. Adam, G. Najafi, R. Mamat, Green fuel as alternative fuel for diesel engine: A review, Renewable and Sustainable Energy Reviews 80 (2017) 694-709.

[9] S. De, R. Luque, Upgrading of waste oils into transportation fuels using hydrotreating technologies, Biofuel Research Journal (2014) 107-109.

[10] T. Kandaramath Hari, Z. Yaakob, N.N. Binitha, Aviation biofuel from renewable resources: Routes, opportunities and challenges, Renewable and Sustainable Energy Reviews 42 (2015) 1234-1244.

[11] F. Ye, Y. Li, Q. Yang, Designing coordination contract for biofuel supply chain in China, Resources, Conservation and Recycling 128 (2018) 306-314.

[12] H.A. Ahmed, A.A. Altalhi, S.A. Elbanna, H.A. El-Saied, A.A. Farag, N.A. Negm, E.A. Mohamed, Effect of Reaction Parameters on Catalytic Pyrolysis of Waste Cooking Oil for Production of Sustainable Biodiesel and Biojet by Functionalized Montmorillonite/Chitosan Nanocomposites, 7(5) (2022) 4585-4594.

[13] A. Alvarez, J. Ancheyta, Modeling residue hydroprocessing in a multi-fixed-bed reactor system, Applied Catalysis A: General 351(2) (2008) 148-158.

[14] S. Bezergianni, A. Kalogianni, I.A. Vasalos, Hydrocracking of vacuum gas oil-vegetable oil mixtures for biofuels production, Bioresource Technology 100(12) (2009) 3036-3042.

[15] S. Bezergianni, S. Voutetakis, A. Kalogianni, Catalytic Hydrocracking of Fresh and Used Cooking Oil, Industrial & Engineering Chemistry Research 48(18) (2009) 8402-8406.

[16] M.A. Callejas, M.T. Martínez, Hydroprocessing of a Maya Residue. II. Intrinsic Kinetics of the Asphaltenic Heteroatom and Metal Removal Reactions, Energy & Fuels 14(6) (2000) 1309-1313.

[17] M.S. El-Sayed, N. Ali, Z. El-Sayed Ali, Aggregation and Activation of Blood Platelets in Exercise and Training, Sports Med. 35(1) (2005) 11-22.

[18] L. Bently, B. Sherman, D. Gangjee, P. Johnson, 16. Procedure for grant of a patent, Intellectual Property Law, Oxford University Press, 2018.
[19] F. Guo, S. Guo, X.-X. Wei, X. Wang, H. Xiang, Z. Qiu, L. Zhao, MCM-41 Supports Modified by Al, Zr and Ti for NiW Hydrodenitrogenation Catalysts, Catalysis Letters 144(9) (2014) 1584-1593.
[20] T. Klimova, L. Peña, L. Lizama, C. Salcedo, O.Y. Gutiérrez, Modification of Activity and Selectivity of NiMo/SBA-15 HDS Catalysts by Grafting of Different Metal Oxides on the Support Surface, Industrial & Engineering Chemistry Research 48(3) (2008) 1126-1133.
[21] T. Klimova, E. Rodríguez, M. Martínez, J. Ramírez, Synthesis and characterization of hydrotreating Mo catalysts supported on titania-modified MCM-41, Microporous and Mesoporous Materials 44-45 (2001) 357-365.
[22] E. Rodríguez-Castellón, A. Jiménez-López, D. Eliche-Quesada, Nickel and cobalt promoted tungsten and molybdenum sulfide mesoporous catalysts for hydrodesulfurization, Fuel 87(7) (2008) 1195-1206.
[23] R. Silva-Rodrigo, C. Calderón-Salas, J.A. Melo-Banda, J.M. Domínguez, A. Vázquez-Rodríguez, Synthesis, characterization and comparison of catalytic properties of NiMo- and NiW/Ti-MCM-41 catalysts for HDS of thiophene and HVGO, Catalysis Today 98(1-2) (2004) 123-129.
[24] M.J.B. Souza, B.A. Marinkovic, P.M. Jardim, A.S. Araujo, A.M.G. Pedrosa, R.R. Souza, HDS of thiophene over CoMo/AlMCM-41 with different Si/Al ratios, Applied Catalysis A: General 316(2) (2007) 212-218.
[25] A.M. Alsabagh, S.S. Selim, M. Elmelawy, M. Ebiad, A.A. ALY, M. Behalob, S.A. Ghoneim, HYDROCRACKING OF OLEIC ACID USING MODIFIED NIW/SZ-MCM-41 TO PRODUCE ECO-FRIENDLY GREEN FUELS, Global Journal of Advanced Engineering Technologies and Sciences 5(5) (2018) 16-29.
[26] H.I. Meléndez-Ortiz, L.A. García-Cerda, Y. Olivares-Maldonado, G. Castruita, J.A. Mercado-Silva, Y.A. Perera-Mercado, Preparation of spherical MCM-41 molecular sieve at room temperature: Influence of the synthesis conditions in the structural properties, Ceramics International 38(8) (2012) 6353-6358.
[27] E. Furimsky, Deactivation of hydroprocessing catalysts, Catalysis Today 52(4) (1999) 381-495.
[28] S. Elbanna, A. Rhman, A. Al-Hussaini, S. Khalil, Synthesis and characterization of polymeric additives based on α-Olefin as pour point depressant for Egyptian waxy crude oil, Petroleum Science and Technology 35 (2017) 1047-1054.
[29] S. Elbanna, A. Rhman, A. Al-Hussaini, S. Khalil, Synthesis, characterization, and performance evaluation of novel terpolymers as pour point depressors and paraffin inhibitors for Egyptian waxy crude oil, Petroleum Science and Technology 40 (2022) 2263-2283.
[30] H.A. Ahmed, S.A. Elbanna, R. Khalil, A. Tayel, A.B. El Basaty, Ultrasonic-assisted Hydrothermal Synthesis of Zeolite Y Adsorbent from Natural Kaolin for the Recycling of Waste Engine Oil, Egyptian Journal of Chemistry 65(131) (2022) 151-160.
[31] H.I. Meléndez-Ortiz, B. Puente-Urbina, G. Castruita-de Leon, J.M. Mata-Padilla, L. García-Uriostegui, Synthesis of spherical SBA-15 mesoporous silica. Influence of reaction conditions on the structural order and stability, Ceramics International 42(6) (2016) 7564-7570.
[32] K.C. Kwon, H. Mayfield, T. Marolla, B. Nichols, M. Mashburn, Catalytic deoxygenation of liquid biomass for hydrocarbon fuels, Renewable Energy 36(3) (2011) 907-915.
[33] B. Rozmysłowicz, P. Mäki-Arvela, S. Lestari, O.A. Simakova, K. Eränen, I.L. Simakova, D.Y. Murzin, T.O. Salmi, Catalytic Deoxygenation of Tall Oil Fatty Acids Over a Palladium-Mesoporous Carbon Catalyst: A New Source of Biofuels, Topics in Catalysis 53(15-18) (2010) 1274-1277.
[34] H.A. Elmawgoud, T.M. Elshiekh, S.A. Elbanna, S.A. Khalil, Modeling and Simulation for Estimating Injection Dose Rate of a Hydrogen Sulphide Scavenger for Treating Natural Gas, Egyptian Journal of Chemistry (2023) -.
[35] M. Jha, A.K. Sinha, P. Agnihotri, Hydroprocessing of Jatropha oil to produce green fuels, International Journal of Chem. Tech. Research 5(2) (2013) 765-770.
[36] H. Heriyanto, S.D. Murti Sumbogo, S.I. Heriyanti, I. Sholehah, A. Rahmawati, Synthesis of Green Diesel From Waste Cooking Oil Through Hydrodeoxygenation Technology With NiMo/γ-Al₂O₃ Catalysts, MATEC Web of Conferences 156 (2018) 03032.
[37] G.C.R. Silva, M.H.C. de Andrade, Simulation of deoxygenation of vegetable oils for diesel-like fuel production in continuous reactor, Biomass Conversion and Biorefinery 13(3) (2021) 1843-1857.
[38] D. Singh, S.S. Sandhu, A.K. Sarma, An investigation of green diesel produced through hydro-processing of waste cooking oil using an admixture of two heterogeneous catalysts, Energy Sources, Part A: Recovery, Utilization, and Environmental Effects 40(8) (2018) 968-976.
[39] X. Zhao, L. Wei, S. Cheng, E. Kadis, Y. Cao, E. Boakye, Z. Gu, J. Julson, Hydroprocessing of carinata oil for hydrocarbon biofuel over Mo-Zn/Al2O3, Applied Catalysis B: Environmental 196 (2016) 41-49.